Hindawi
Modelling and Simulation in Engineering
Volume 2023, Article ID 6128517, 19 pages
https://doi.org/10.1155/2023/6128517

Research Article

Mathematical-Based CFD Modelling and Simulation of Mushroom Drying in Tray Dryer

Talbachew Tadesse Nadew,[1] **Petros Demissie Tegenaw**,[2] **and Tsegaye Sissay Tedila**[3]

[1]*Department of Chemical Engineering, College of Mechanical and Chemical Engineering, Wollo University, Kombolcha Institute of Technology, Kombolcha, Ethiopia*
[2]*Department of Electromechanical Engineering, Faculty of Engineering Technology, KU Leuven, 3000 Leuven, Belgium*
[3]*Department of Chemical Engineering, College of Biological and Chemical Engineering, Addis Ababa Science and Technology University, Addis Ababa, Ethiopia*

Correspondence should be addressed to Talbachew Tadesse Nadew; talewtadesse4897@gmail.com

Received 29 April 2023; Revised 27 September 2023; Accepted 3 October 2023; Published 26 October 2023

Academic Editor: Andrea Maranzoni

In this study, CFD simulations that incorporate the inherent coupling between the moisture content of the mushroom and hot air flow in the tray dryer were performed. Conservation principles were applied to the fundamental quantities of mass, momentum, and heat. The source terms due to the moisture evaporation, the viscous and inertial resistance, and continuous evaporative cooling were determined through experimental results. Experiments were conducted to study and select the drying kinetics model at the optimum drying conditions and moisture sorption isotherm model at 30, 40, and 50°C temperatures. The best model describing the drying kinetics of mushrooms and moisture sorption isotherm model was chosen based on the lowest RMSE values and the highest R^2 value. Midilli et al.'s drying kinetics model and the modified Henderson sorption isotherm model were adopted in CFD modelling. The CFD software *ANSYS* Fluent was used for the 3D modelling of mushroom drying in a tray dryer. The mass and energy source term equations were added to the ANSYS Fluent software using a user-defined function (UDF). The parameter permeability of medium (α) and pressure-jump coefficient (C_2) appearing in the momentum source term were directly introduced in the Fluent setup as cell zone conditions. The simulation results of the moisture removal and drying temperatures were validated against experimental data. Both results are in good agreement with the experimental data, with R^2 values of 0.9906 for moisture contents and 0.926 for drying temperature. Thus, simulation can be an option to study the drying mechanisms and alleviate some drawbacks of doing experiments.

1. Introduction

All food items in our daily life must be preserved in some way. Mushroom is highly nutritious, delicious, and safe to eat, but it is highly perishable because it has a moisture content in the range of 85-95% by weight (wt) when wet and has a very short shelf life [1]. Harvested mushroom can remain in atmospheric condition for up to one day only without rotting [2]. For this reason, processes that suppress product deterioration have become an important issue. The most common methods of preserving food, such as mushrooms and fruits, are long-term preservation methods, such as canning, pickling, drying, and adding chemicals [3, 4]. Drying is the most common method of preserving food and shows promise for preserving moist foods and other agricultural products [5].

Therefore, the drying of food products, such as mushrooms, meat, and fruits, is carried out to preserve their desired nutritional properties for as long as possible, thus facilitating their transport, storage, and handling [6, 7]. Many drying techniques can be used for mushroom drying such as sun drying, vacuum drying, microwave drying, freeze-drying, and tray drying. When tray drying is applied, the moisture content in the mushroom should be removed at some optimum conditions. The drying process depends on the moisture content inside the material, drying temperature, drying medium, and time. Therefore, the drying process should be optimized to save energy and to keep the important nutrients in the drying process, especially for mushroom drying [8, 9]. The experimental processes of drying such as the measurement of temperature distribution, mass flow, and velocity of air in the tray dryer chamber are expensive, difficult, and time-consuming. Even only partial information will be obtained from the experimental result. This is because it requires many installed sensors and must be adjusted in several parts of the dryer other than inlet and outlet measuring sensors. On top of that, most industrial dryers are designed based on expensive pilot-scale experiments [10]. The complexity of the drying process due to the diverse nature of the material being dried hinders the development of a global drying model that can be used for various tray dryer designs under different operating. Since the cost of experimental testing can be substantial, theoretical analyses of these drying systems at the design and modelling stage can reduce the cost largely, while producing a better understanding of the process with detailed analyses [11].

Recently, there have been many pieces of research on the mathematical modelling and experimental studies of the drying characteristics of various vegetables and fruits, such as grapes [12], apples [13], peaches [14], carrots [15], beriberi [16], and potatoes [17]. Some work has been reported to dry mushroom and extend shelf life using various post-harvest techniques. However, there are sparse studies in the literature on computer-aided modelling techniques for mushroom drying in tray dryers [3, 18]. Moreover, previous modelling attempts were limited to mathematical modelling and whole-food drying processes.

In the last decade, Arumuganathan et al. [5] developed a model for a fluidized bed dryer for drying milky mushroom by taking into account only the mass transfer during drying. Nevertheless, to my knowledge, there was no computational fluid dynamics (CFD) model for drying mushroom by considering the simultaneous heat and mass transfer during drying. Effective modelling and simulation of the tray dryer system may eliminate or reduce the nonuniformity of drying and increase dryer efficiency. This paper discussed the optimization of drying parameters, CFD modelling, and simulation of a tray dryer system for drying mushroom by using an appropriate modelling approach. CFD simulation is a very useful tool in the optimization of the drying chamber configuration by predicting the airflow distribution and the temperature profile throughout the tray-drying chamber [19, 20]. This is very important for many food industries and research institutes (laboratories) since it reduces the number of experiments saving time and money.

2. Materials and Method

2.1. Materials. The raw materials used in this research was oyster mushroom collected from Menagesha Integrated Organic Farm mushroom harvesting company, Holeta, Addis Ababa, Ethiopia.

2.2. Experimental Methods

2.2.1. Sample Preparation. Freshly harvested oyster mushrooms were washed several times with water to remove dust and impurities. After draining, mushrooms were covered with blotting paper to remove surface moisture. Then, cleaned mushroom having flat shapes were cut into small slices with an average rectangular dimension of 26 mm × 13 mm using a slicer to increase the moisture removal rate. The slices of mushroom samples were kept in a refrigerator at 4°C to keep the moisture content until used for further processing.

2.2.2. Oyster Mushroom Drying Process Using Tray Dryer. Drying was performed in a hot air-drying medium of a computer-controlled tray dryer (CCTD/SCADA, Edibon, Italy). The dryer mainly consists of four basic units (1) an air compressor, (2) an air velocity regulator, (3) an electrical heater, and (4) a drying chamber (tray). The drying chamber had four trays made up of stainless steel with 270 mm by 240 mm dimensions. The compressor blew air into the heater; the hot air was blown to the tray horizontally; and then the hot air removed the moisture from the sample. The tray dryer used in this study is presented in Figure 1. A known amount of sample in grams (w_0) was placed on the tray, and the temperature and air speed were set within the range of 40–80°C and 0.5–5.5 m/s, respectively. Then, the sample weight was continuously recorded and used to estimate the amount of moisture removed during drying as per the following equation:

$$M_{\mathrm{DS}}(wt\%) = \frac{W_{Mi} - W_{Mt}}{W_{Mi}} \times 100\%, \tag{1}$$

where M_{DS}, W_{Mi}, and W_{Mt} are the amount of moisture present in a dried sample, the amount of moisture present in a fresh sample, and the amount of moisture removed at some time t, respectively.

2.2.3. Determination of Initial Moisture Content and Dry Weight. The fresh mushroom sliced was weighed by using an electronic balance (AD-300-3, USA) and put in an oven (700LT-model no. TD-1315, Cooper Technology, UK) set at 105°C for 24 hrs. About 0.2 kg sample was taken in a tray and weighed again accurately to give the exact weight of the sample. The residual weight after 24 hours was used as the dry weight (w_d) of the mushroom. To obtain the initial moisture content (MC), equation (2) was used.

$$\mathrm{MC}(wt\%) = \frac{W_o - W_d}{W_o} \times 100, \tag{2}$$

where w_0 is the initial weight of the mushroom sample and w_d is the dry weight of the sample.

2.3. Parameter Optimization for Mushroom Drying in a Tray Dryer. The preliminary experiments were conducted with a drying period of eight hours by considering drying temperature (40–80°C), hot drying air speed (1–5.5 m/s), and mass load (50–500 g) as parameters, and the individual effect has been investigated on the moisture content of the final product. Based on the preliminary experimental results, the upper and lower limits for temperature, hot air speed, and mass loading were fixed to obtain the experimental matrix to investigate the interaction effect between these drying

Figure 1: Computer-controlled tray dryer used in this study.

Table 1: Experimental matrix for design-expert in oyster mushroom drying.

Process parameters	Labels	Units	Lower value	Higher value
Temperature	T	°C	50	70
Hot air speed	V	m/s	2	5
Mass of mushroom slice	W	G	100	300

parameters on the drying of oyster mushroom listed in Table 1. A design expert was used to optimize the parameters for mushroom drying [21].

Numerical optimization was performed for three parameters (temperature, hot air speed, and mass of mushroom) to minimize moisture in oyster mushroom during tray dryer. The optimum drying parameters obtained from the optimization process were further used to study mushroom drying kinetics and in the CFD model simulation steps. The interaction between the parameters of the drying process is fitted with the following equation:

$$Y = \beta_0 + \beta_1 x_1 + \beta_2 x_2 + \beta_3 x_3 + \beta_4 x_1 x_2 + \beta_5 x_1 x_3 + \beta_6 x_2 x_3 + \beta_7 {x_1}^2 + \beta_8 {x_2}^2 + \beta_9 {x_3}^2 + \xi, \tag{3}$$

where Y is the response function (moisture content), $\beta_0 - \beta_9$ are regression coefficients, x_1, x_2, and x_3 are the independent parameters, and ξ is the error [22].

2.4. CFD-Based Modelling for Mushroom Drying in Tray Dryer. The CFD model is based on the fundamental conservation equations of mass, momentum, and energy. The source terms (mass during moisture evaporation, momentum due to viscous and inertial resistance of mushroom, and energy due to the continuous cooling evaporation process) were not included in the conservation equations of the CFD software package (ANSYS 2020R$_1$). The source terms for the three quantities were derived and determined from the experiments. All the parameters and physical properties required to build the model were obtained from the literature and direct experimental results of drying experiments.

2.4.1. Source Term Determination

(1) Mass Source Term Determination. The conservation of air mass when the mushroom was drying is given in equation (4) [23–25].

$$\frac{\partial \rho}{\partial t} + \nabla . \left(\rho \vec{V}\right) = S_m, \tag{4}$$

where ρ is the density of the fluid (air), $\vec{V}$ is the velocity vector, and S_m is the mass source term.

The source S_m is the mass added to the continuous phase (drying air) from the second phase (porous medium) due to vaporization moisture from the mushroom slices. S_m can be expressed similarly to Fick's second law of diffusion as per equation (5) as suggested by Thorpe [23].

$$S_m = -(1-\varepsilon)\rho_m \frac{dMt}{\mathrm{dt}}, \tag{5}$$

where ρ_m is the density of the mushroom and ε is the porosity of the sliced mushroom.

(2) External/Bulk Porosity ($\mathcal{E}_b$). The porosity of the slices of mushroom was calculated using the expression given in the following equation:

$$\mathcal{E}b = \frac{\text{Volume of empty space (i.e total volume minus occuppied volume by sample)}}{\text{total volume of sample holder}} = \frac{Vt - Vs}{Vt}, \tag{6}$$

where Vt is the total volume (length × width × height) of the sample holder and Vs (volume of samples) is equal to the volume of a single slice multiplied by the total number of slices.

(3) Momentum Source Determination. Conservation of momentum is described in equation (7) as discussed in [25].

$$\frac{\partial}{\partial t}\left(\rho \vec{V}\right) + \nabla \cdot \left(\rho \vec{V} \vec{V}\right) = -\nabla P + \nabla \cdot \bar{\bar{\tau}} + \rho \vec{g} + \vec{s_i}, \tag{7}$$

where P is the static pressure, $\bar{\bar{\tau}}$ is the stress tensor, and $\rho\vec{g}$ and $\vec{s_i}$ are the gravitational body force and external body force (i.e., it may be from the interaction with the dispersed phase), respectively. $\vec{s_i}$ also contains other model-dependent source terms, such as porous media and user-defined momentum sources. In the tray dryer case, the hot air flow is horizontal. Then, this momentum source term was determined through the following equation:

$$s_i = \frac{dP}{\mathrm{dx}} = -\left(\frac{\mu}{\alpha}v + \frac{c_2}{2}\rho_{\mathrm{air}}v^2\right), \tag{8}$$

where α is the permeability, C_2 is the inertial resistance factor, and v is the velocity of air in the horizontal direction. α and C_2 were determined using Ergun's equation (9), as suggested by [26–28].

$$\frac{\Delta p}{L} = \frac{150(1-\varepsilon)^2\mu v}{\phi^2\varepsilon^3\mathrm{Def}^2} + \frac{1\cdot 75(1-\varepsilon)\rho v^2}{\phi\varepsilon^3\mathrm{Def}}, \tag{9}$$

where $\alpha = 0.00667Def^2\varepsilon^3/(1-\varepsilon)^2$, $C_2 = (3.5/Def)((1-\varepsilon)/\varepsilon^3)$, and D_{ef} is the effective diameter of mushroom slices and ε is the porosity. For spherical particles, ϕ in equation (9) is equal to unity.

(4) Effective Diameter (D_{ef}) of Mushroom Slices. The shapes of different mushroom species are irregular. To determine the effective diameter of the mushroom slices, liquid water is used in a measuring cylinder filled with an initial volume of 60 ml. After the slices of mushroom were immersed, the resulting volume differences observed between the water volumes with slices and without slices were taken, and the D_{ef} of the sliced mushroom was calculated, exploiting the formula of the sphere volume, as

$$v_{sphere} = \frac{4}{3\pi(\mathrm{Def}/2)^3 = v_f} - v_0, \text{ then } Def = 2\left(\sqrt[3]{\frac{3}{\pi}\left(v_j - v_0\right)}\right). \tag{10}$$

(5) Energy Source Determination. Energy conservation equation was determined as described in reference [25].

$$\frac{\partial}{\partial \mathrm{t}}(\rho \mathrm{E}) + \nabla\cdot\left(\vec{\mathrm{V}}(\rho\mathrm{E} + \mathrm{p})\right) = \mathrm{s_h}, \tag{11}$$

where E is the total energy. The first three terms on the left-hand side of the equation represent energy transfer due to conduction, species diffusion, and viscous dissipation, respectively. s_h is the energy source term, which is due to the effect of evaporative cooling. This was determined using the expression in equation (12) as reported in reference [23]:

$$s_h = -h_{\mathrm{fg}}(1-\varepsilon)\rho_m\frac{\partial M}{\partial \mathrm{t}}, \tag{12}$$

Table 2: Different mathematical models for describing drying kinetics.

Model name	Model	References
Lewis or Newton	MR = exp (-kt)	[40]
Page	MR = exp $(-\mathrm{kt}^n)$	[41]
Modified page	MR = exp $(-\mathrm{kt})^n$	[41]
Two exponentials	MR = a exp $(-kt)$ + $(1-a)$ exp (−kt)	[42]
Henderson and Pabis	MR = a exp (−kt)	[43, 44]
Logarithmic	MR = a exp (−kt) + c	[42]
Midilli et al.	MR = a exp (kt^n) + bt	[45]
Singh et al.	MR = exp (−kt) − akt	[46]

Table 3: Different moisture sorption models selected for mushrooms.

Names	Model equation	Reference
Modified Chung and Pfost	$Me = -\frac{1}{C}\ln\left(-\left(\frac{T+B}{A}\right)\ln a_w\right)$	[47]
Iglesias and Chirife	$Me = A\left(\frac{a_w}{2-a_w}\right) + B$	[48]
Modified Henderson	$Me = \left(-\frac{\ln(1-a_w)^{1/C}}{A(T+B)}\right)$	[49]
GAB	$Me = \left(\frac{M_0\mathrm{CK}a_w}{(1-Ka_w)(1-Ka_w+\mathrm{CK}a_w)}\right)$	[50]
BET	$\frac{a_w}{((1-a_w)Me)} = A + Ba_w$	[51]
Modified Halsey	$Me = \frac{1}{c}\ln\left(\frac{(-e)^{(A+B)}}{\ln(a_\omega)}\right)$	[52]
Ferro-Fontan	$Me = \left[-\frac{1}{A}\ln\frac{B}{a_w}\right]^{1/C}$	[53]

where h_{fg} is the latent heat of vaporization, which was calculated, for the range of temperature 0 to 260°C, from the relation [29].

$$h_{\mathrm{fg}} = 250300 - 2386(T - 273.15), \tag{13}$$

where T is the temperature expressed in K. Substituting the expression for $\partial M/\partial \mathrm{t}$ obtained from mass source determination and equation (13) into equation (12), the heat source term was determined.

2.4.2. Drying Kinetics Models. A mass of mushrooms of 200 g was dried at six different temperatures (50, 55, 60, 65, 70, and 75°C) with a hot air speed of 3 m/s. The weight percent moisture content (w_b) was recorded at 15-minute intervals and used to study the mushroom drying rate. The moisture

Table 4: Dimension of the tray dryers, trays, and mushroom slices.

Dimensions	Units	Values
Tray dryers Box part $(L \times W \times H)$	mm	$1000 \times 320 \times 320$
Tray dryer pyramidal part $(X.Y.Z)$	mm	$400 \times 160 \times 160$
Tray $(L \times W \times H)$	mm	$270 \times 240 \times 15$
Mushroom slices × number of slices	mm	$(25.8 \times 12.9 \times 25.8) \times 180$

content remaining in the samples was plotted against time at various temperatures [30, 31]. The dimensionless ratio of moisture content difference (MR) is defined by [32–34].

$$\mathrm{MR} = \frac{Mt - Me}{Mo - Me}, \tag{14}$$

where Mt, Me, and Mo are the moisture content at a time t, the equilibrium moisture content, and the initial moisture content, respectively.

Then, the mushroom drying rate was obtained by the time derivative of MR.

$$\frac{dMt}{dt} = \frac{d\mathrm{MR}}{dt}(Mo - Me). \tag{15}$$

Me changes with the moisture content of mushroom slices. So, Me has been determined from the moisture sorption isotherm model (see section 2.4.3).

In this study, the experimental data were fitted with eight selected well-known thin-layer drying kinetics models listed in Table 2. The model parameters were estimated through a non-linear regression method using a MATLAB script (MATLAB R2018b). The fitting quality of the experimental data for all selected models was evaluated using the coefficient of determination (R^2) and the root means square error (RMSE). The best model describing the drying kinetics of mushrooms (showing the lowest RMSE value and the highest R^2 value) was selected to determine the source term.

2.4.3. Moisture Sorption Models. The remaining term to be determined is the equilibrium water content Me, which can be determined from the water sorption model. Food sorption isotherms describe the thermodynamic relationship between water activity and the equilibrium water content of food at constant temperature and pressure [35]. Seven selected sorption models were tested and the one with the good-of-fit was used in the modelling (Table 3). Water activity (a_w) experiments were done to select the sorption model using water activity meters (AQUA LAB: 4TE, Italy), which measure the water activity of mushrooms when the moisture content reached equilibrium at a given temperature. a_w vs. equilibrium moisture content data was generated at temperatures of 30, 40, and 50°C. The goodness-of-fit of the model was determined with a higher value of R^2 and lower values of RMSE.

After the model is selected, the water activity of the sample is related to the absolute humidity and relative humidity of the drying medium [23, 29] through the following equation:

Table 5: Boundary conditions and parameters used in the simulations.

Parameters	Units	Values
Mushroom density	$\mathrm{Kg/m^3}$	769
Air inlet velocity	m/s	3
Density of air	$\mathrm{Kg/m^3}$	1.225
Air inlet temperature	°C	60
Porosity of sample	%	0.38
Material constructions	Stainless steel	
Thermal conductivity of mushroom	W/m. K	0.37438
Specific heat capacity of mushroom	KJ/Kg. K	2.960
Thermal conductivity of air	W/m. K	0.022
Specific heat capacity of air	KJ/Kg. K	1.005

$$a_w = \frac{RH}{100}, \tag{16}$$

where RH is the relative humidity of drying air and is related to the absolute humidity (AH) as

$$\mathrm{AH} = \frac{0.622 \times \mathrm{RH} \times P_{\mathrm{sat}}}{(P_{\mathrm{atm}} - (\mathrm{RH} \times P_{\mathrm{sat}}))}, \tag{17}$$

where P_{sat} is the saturation vapor pressure of free water, which is a function of the absolute temperature. In this study, P_{sat} was determined using the Antione equation for free water [36] as

$$P_{\mathrm{sat}} = \exp\left(16.59 - \frac{3643.31}{(T_{\mathrm{abs}} + 33.42)}\right), \tag{18}$$

where T_{abs} is the absolute temperature. Finally, the rate of drying dMt/dt was obtained as a function of absolute humidity, moisture content, temperature, and drying time.

2.5. CFD Modelling. The CFD-based model for drying mushrooms was implemented to capture the moisture and temperature variation of the mushroom during drying. The ANSYS Fluent has a conserved Navier-Stokes equation for the fundamental quantities of the mass, momentum, and energy, whereas the source terms were not included in the conservation equations of CFD software package. These terms were determined and added to the ANSYS Fluent package by developing a user-defined function (UDF) written in C-program using the *Code::Blocks* software which is compatible with ANSYS Fluent.

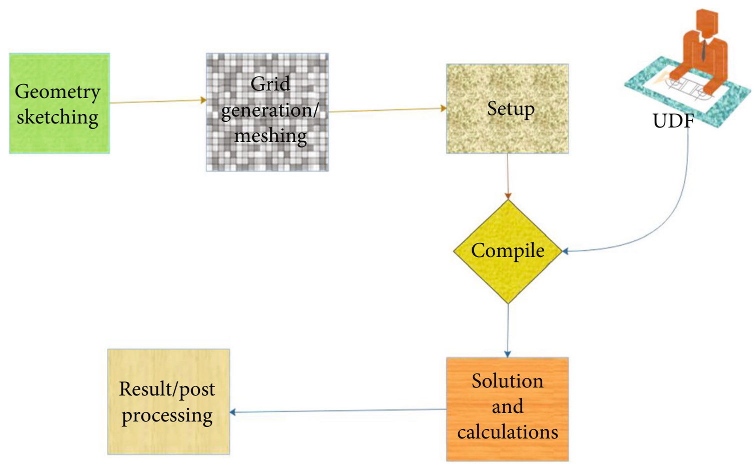

Figure 2: General procedure of CFD simulation.

Table 6: Optimal value of drying parameters and experimental response at optimum condition.

Parameter and response	Range	Optimum moisture content (wt%)		Deviation
		Model	Experimental	
Temperature (°C)	(50, 70)	60	59.81	0.19
Airspeed (m/s)	(2, 5)	3	2.96	0.04
Mass of slice mushroom (g)	(100,300)	200	200	0
Moisture content (wt%)	10	9.99	10	0.01

2.5.1. Geometry and Meshing. In ANSYS Fluent, the DesignModeler was used to draw the geometry of the tray dryer (fluid domain) and the mushroom slices. The fluid domain was made symmetric to minimize the simulation time, and due to computational cost, the mushroom slices were considered as a large rectangular slice. The dimensions of the tray dryer, tray, and mushroom slices are given in Table 4 from the specification and measurement of actual dimensions at the laboratory.

A tetrahedron meshing method was used in the grid generation because it produced a good mesh with skewness less than 0.95 [25]. To reduce simulation time, a 0.003 m mesh size was used. An additional inflation layer was applied to capture the near-wall flow variables in the boundary layer region. To define the thickness of the first layer, an online $Y+$ calculator was used and found 0.0009 m. $Y+$ expresses the distance from the wall to the center of the first grid cell. The boundary layer was inflated to 24 layers at a growth rate of 1.2. The air inlet, outlet, symmetry surface, walls, and fluid domain were defined after the mesh was generated. The mushroom slices were modelled as porous media.

2.5.2. Setup and Solutions. In the physics setup, double precision for better accuracy was selected. The solver was pressure-based steady state for fluid flow only, and transient simulations after UDF were compiled. The mushroom slice was considered a solid and was created in the materials list; then, it was modeled as a porous media. First, viscous (realizable $k-\varepsilon$ and $k-\omega$ shear-stress transport (SST)) turbulent models have been used to solve the flow without source terms. Then, the two turbulence models were compared based on their wall $Y+$ values. The wall $Y+$ is used as guidance in selecting the appropriate grid configuration and corresponding turbulence models in Fluent [37]. Energy was activated in the Fluent physics setup after the steady flow simulation converged. All material properties and boundary conditions are given in Table 5. Convergence criteria for all residuals were set, and standard initialization was used. More than 2000 iterations were made with a fixed 0.01 sec time-step.

2.5.3. UDF: User-Defined Functions. UDFs (S_m and S_h) were written in the C-programming language using *Code::Blocks* and were defined using *DEFINE* macros provided by ANSYS Fluent. Three general macros are used to develop the UDF for mushroom drying: the macro *DEFINE_INIT (name, d)* to specify the initial value of the parameters and variables; the macro *DEFINE_ADJUST (name update, d)* to update the moisture value at every time-step at each element; and the macro *DEFINE_SOURCE (name, d)* to specify the mass and energy source terms. The coefficients (α and C_2) of the S_i term were calculated and fed to the porous zone in the cell zone conditions. Source files containing UDFs were compiled into ANSYS Fluent (the detail of UDF is given in supplementary file (available here)). Finally, the simulation results were analyzed using contours, streamlines, graphs, and animations. The simulation procedure was sketched in Figure 2.

2.6. Comparison of Simulation and Experimental Results. The simulation result was validated against the experimental data from the tray dryer. In this study, the simulation results

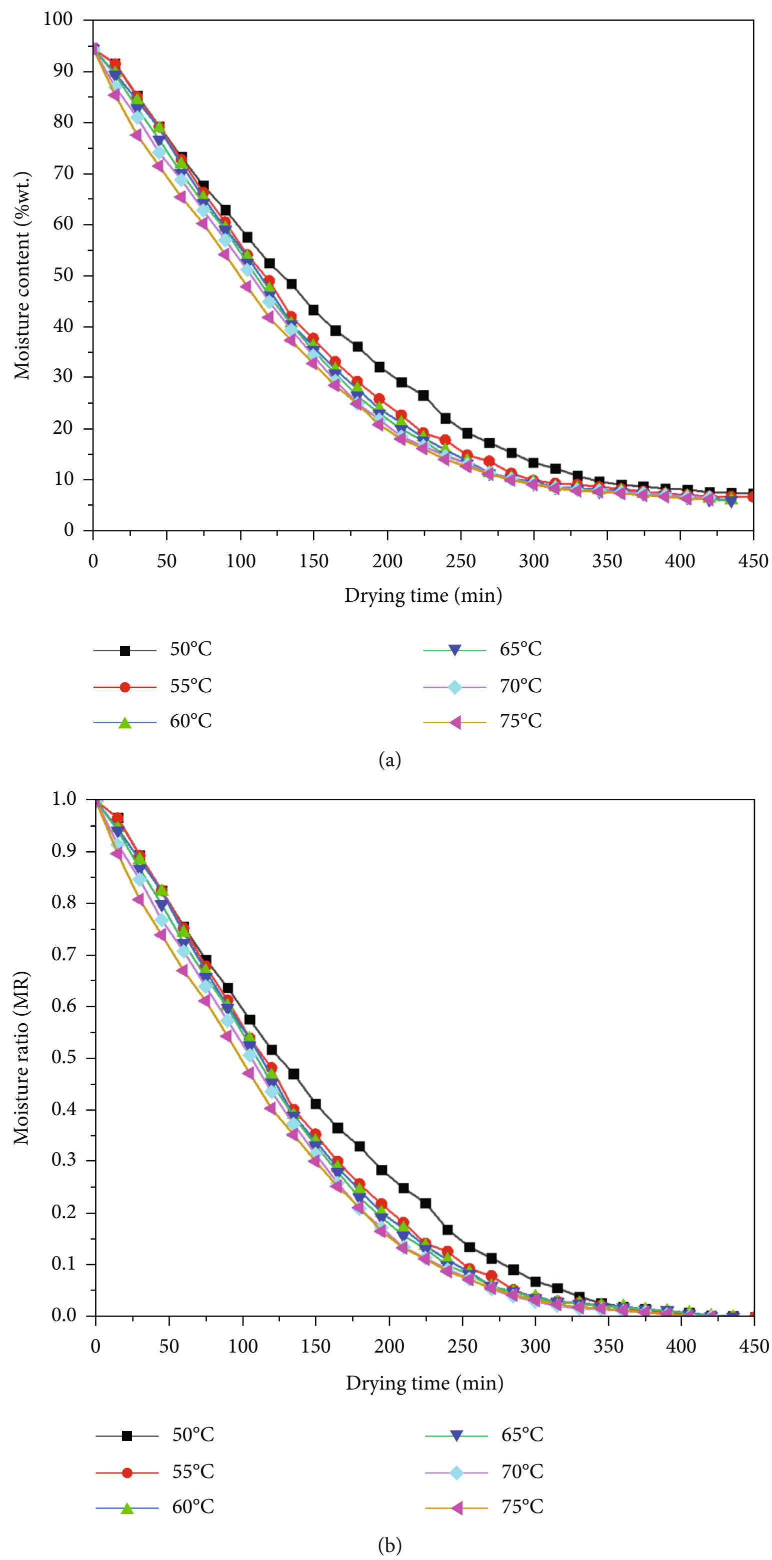

FIGURE 3: Drying curves showing (a) moisture content and (b) moisture ratio dependence on temperatures.

of moisture content and drying temperature on the porous media were compared with the experimental data of the temperature distribution on the porous media and moisture removal rate from the mushroom [38].

3. Results and Discussions

3.1. Optimized Parameters for Oyster Mushroom Drying. Determination of optimal parameter values to dry mushroom

Table 7: Models parameters and goodness of fit for drying kinetics of oyster mushroom at 60°C.

Thin-layer drying models	Coefficients					Statistical values	
	a	*b*	*c*	*k*	*n*	R^2	RMSE
Lewis or Newton	NA	NA	NA	0.008239	NA	0.9804	0.0435
Page models	NA	NA	NA	0.001745	1.31	0.9985	0.01225
Modified page	NA	NA	NA	-0.0668	-0.123	0.9804	0.04427
Two-term exponentials	0.1304	0.9459	NA	0.008813	NA	0.9858	0.03829
Henderson and Pabis	1.076	NA	NA	0.008812	NA	0.9858	0.0376
Logarithmic	1.123	NA	-0.0793	0.007186	NA	0.9945	0.02387
Midilli et al.	0.989	-0.01303	NA	0.001546	1.322	0.9993	0.00875
Singh et al.	0.02528	NA	NA	0.007291	NA	0.9914	0.02932

NA = not applicable.

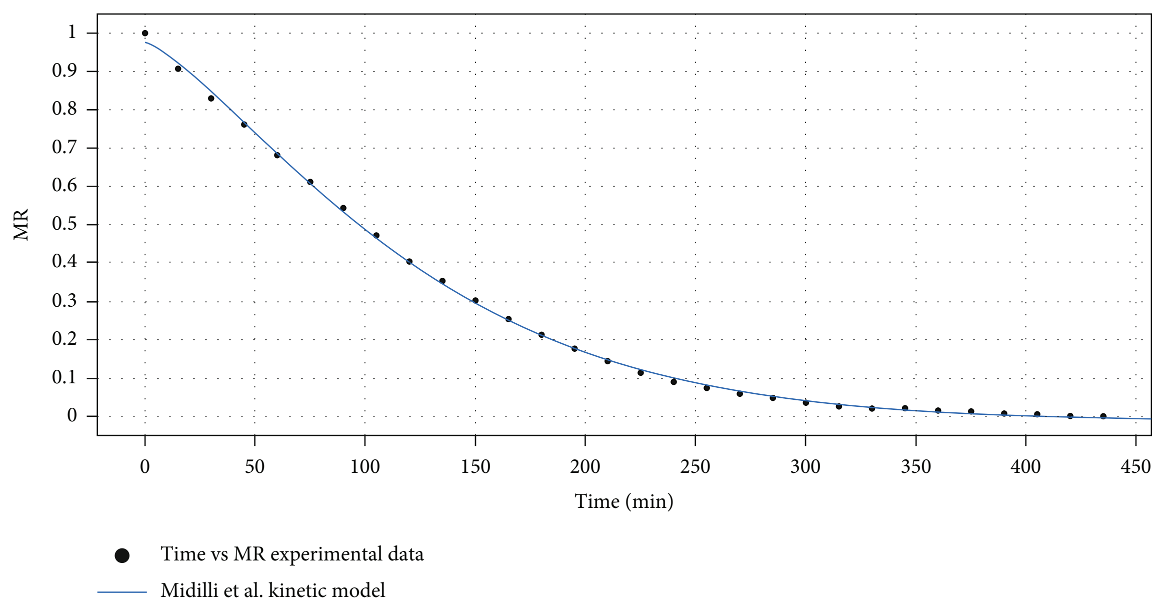

Figure 4: Nonlinear regression based on the Midilli et al. model.

using a tray drier in a hot air-drying medium with three parameters (temperature, drying airspeed, and mass loading of slice mushroom) was conducted. To achieve the desired moisture content of 10 wt%, numerical optimization was done and validated with experiments as indicated in Table 6. The optimum drying temperature, drying airspeed, and mass of the sliced mushroom were 59.81°C, 2.96 m/s, and 200 g, respectively, according to the fitted model numerical optimization performed using a design expert. This gave a moisture content of 9.99 wt% at which the major component of mushroom was well deserved, and the mushroom has a longer shelf life [30]. The interaction between the parameters of the drying process in terms of coded factors was given in the following equation:

$$\begin{aligned}\mathrm{MC(wt\%)} = {} & 9.67 - 4.56A - 1.47B + 3.40C + 2.72AB \\ & + 0.7425AC - 1.47\mathrm{BC} + 3.56A^2 + 3.45B^2 \\ & + 2.99C.\end{aligned} \tag{19}$$

3.2. Modelling and Source Term Determination

3.2.1. Drying Kinetics and Moisture Sorption Models

(1) Drying Kinetics Model. The drying curves of oyster mushroom (MC vs. *t* and MR vs. *t*) at different temperatures using a tray dryer are presented in Figures 3(a) and 3(b), respectively. As can be seen in Figure 3(a), the drying rate increased when drying temperatures rose from 50°C to 55°C. At higher temperatures, the moisture loss is quick, especially in the first 150 minutes (from 93 to roughly 30 wt%). According to this, there was a dropping rate period (i.e., moisture removal is fast) from the start to the first 300 minutes, and then a steady rate period (almost all the moisture is removed) was noticed till the end. A similar tendency is demonstrated in the plot of moisture ratio vs. time at each drying temperature (Figure 3(b)), where faster moisture removal is connected to a higher temperature. The models were evaluated as a function of the moisture ratio and drying time. A nonlinear regression method (implemented in MATLAB) was used to fit the

Table 8: Moisture sorption model constants and statistical parameters.

Sorption models	T (°C)	Coefficients			Statistical parameters	
		A	*B*	*C*	R^2	RMSE
Modified Halsey	50	2.588	0.002258	1.742	0.6679	17.42
	40	-5.346	0.2193	3.464	0.6194	17.13
	30	0.1407	0.1105	3.406	0.6103	17.01
Modified Chung and Pfost	50	4.909	0.0004011	0.1039	0.9184	8.633
	40	5.656	0.0002936	0.08017	0.9406	6.765
	30	5.157	0.0004713	0.08761	0.9462	6.323
Iglesias and Chirife	50	91.13	4.291	AN	0.9532	6.361
	40	96.8	-0.308	NA	0.9654	5.042
	30	95.82	0.2115	NA	0.967	4.845
Modified Henderson	50	-0.000952	-43.8	1.36	0.9762	4.664
	40	-0.004215	-37.53	1.228	0.9891	2.895
	30	-0.001588	-24.1	1.252	0.9871	3.093
GAB	50	$C = -2.314e + 05$	$K = 0.8854$	$Mo = 16.56$	0.9707	5.174
	40	$C = -1.524e + 05$	$K = 0.8897$	$Mo = 16.34$	0.9782	4.102
	30	$C = -2.546e + 05$	$K = 0.8857$	$Mo = 16.77$	0.9687	4.819
BET	50	-0.005688	0.1251	NA	0.7527	13.49
	40	-0.005692	0.1251	NA	0.7527	13.49
	30	-0.003156	0.1174	NA	0.7294	13.88
Ferro-Fontan	50	4.909	0.0004011	0.1039	0.9184	8.633
	40	5.656	0.0002936	0.08017	0.9406	6.765
	30	5.157	0.0004713	0.08761	0.9462	6.323

NA = not applicable.

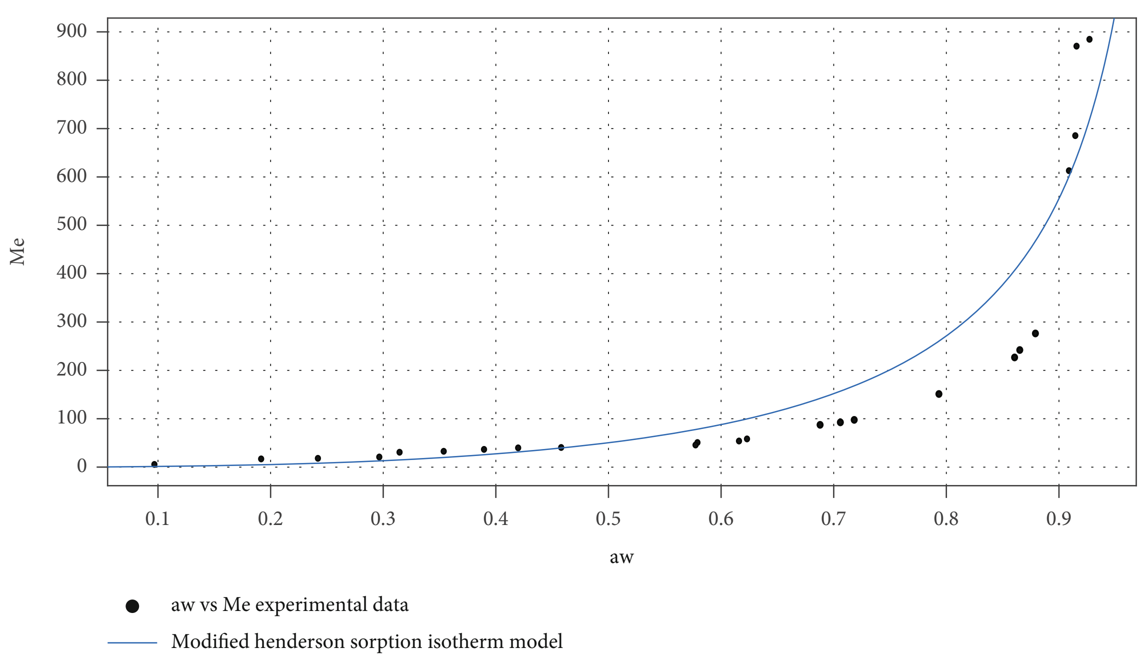

Figure 5: Nonlinear regression curve for modified Henderson sorption isotherm model at 40°C.

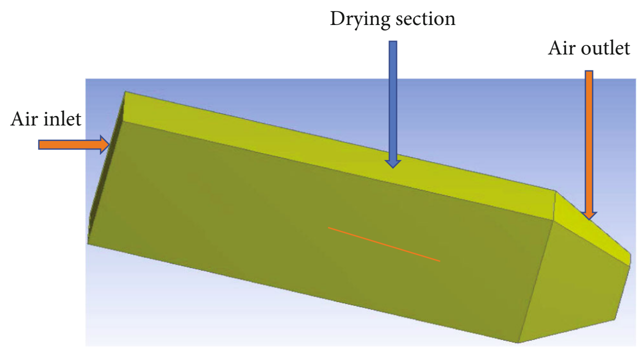

Figure 6: Geometry of tray dryer showing the main parts of dryer.

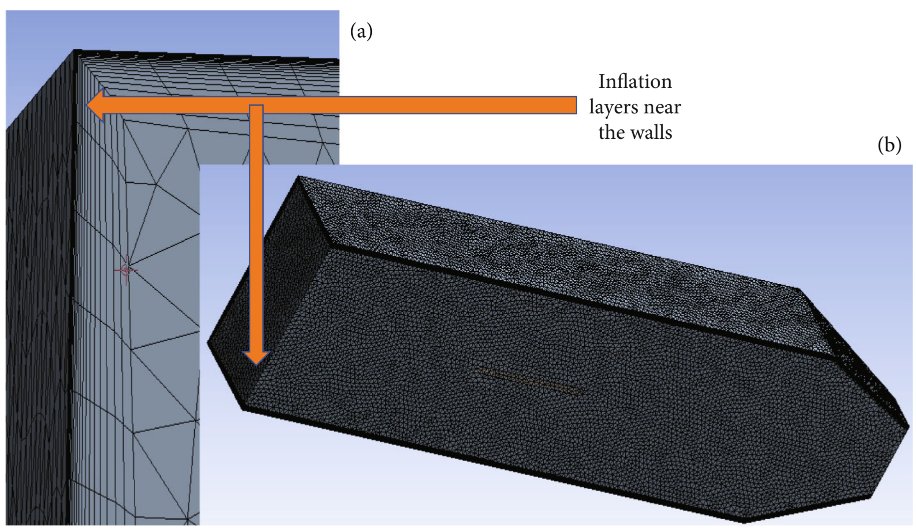

Figure 7: Detail of the computational grid (a) and inflation layer in the near wall (b).

calculated data. Drying kinetics model parameters and related goodness of fit are reported in Table 7 along with statistical values of R^2 and RMSE.

For 60°C, the Midilli et al. drying kinetic model is the best-fit drying kinetics model with $R^2 = 0.9993$ and RSME $= 0.008749$ (Table 7). It was described by Midilli et al. as the best-fit drying model for mushrooms [33]. So, Midilli et al.'s model is the selected model for determining the source term for CFD models. The moisture ratio vs. time curve fit for the Midilli et al. model is shown in Figure 4.

(2) Moisture Sorption Isotherm Model. The moisture sorption isotherm model, which correlates a_w and EMC of the mushroom, was evaluated by comparison with the experimental results. The experimental data at 30, 40, and 50°C and the nonlinear regression curve fitting for sorption isotherm models were studied. The constant coefficients and statistical parameters from the nonlinear regression for sorption Isotherm models are presented in Table 8. The best-fitted model is the modified Henderson sorption model with $R^2 = 0.9891$ and RMSE $= 2.895$ at 40°C. The regression curve based on the modified Henderson model is shown in Figure 5.

Then, the modified Henderson model $Me = (-\ln (1 - a_w))^{1/C} / A(T + B))$ is selected to deal with the moisture sorption of oyster mushroom species, where A, B, and C are model parameters with values -0.004215, -37.53, and 1.228, respectively, and a_w is the water activity ($a_w = \mathrm{RH}/100$), RH being the relative humidity.

(3) Bulk Porosity (Ɛ) and Effective Diameter (D_{ef}) of Mushroom Slices. The external bulk porosity of the sample was found to be 0.388, which is 61% of the tray surface covered by the mushroom slices. The average value of D_{ef} of the mushroom slices was calculated from the difference of volumes of water with mushroom slice and without mushroom and is $25.8 \pm 1.5 \times 10^{-4}$ mm.

(4) Source Term Expression Determination. By combining the drying kinetics model (Midilli et al. model) and the moisture sorption model (modified Henderson model), equation (20) was obtained.

$$\frac{dMt}{\mathrm{dt}} = (M_0 - Me)\left(\left(-\mathrm{aknt}^{n-1}\right)\right)\left(\exp\left(\left(-\mathrm{kt}^n\right)\right) + b\right), \quad (20)$$

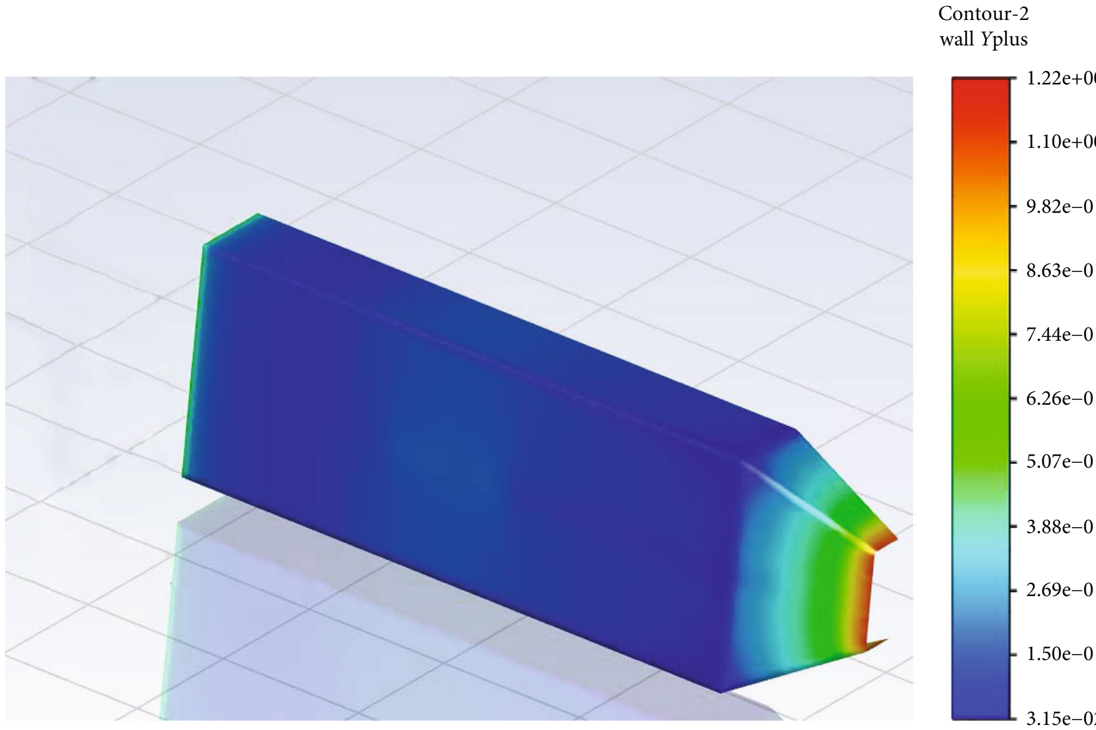

(a)

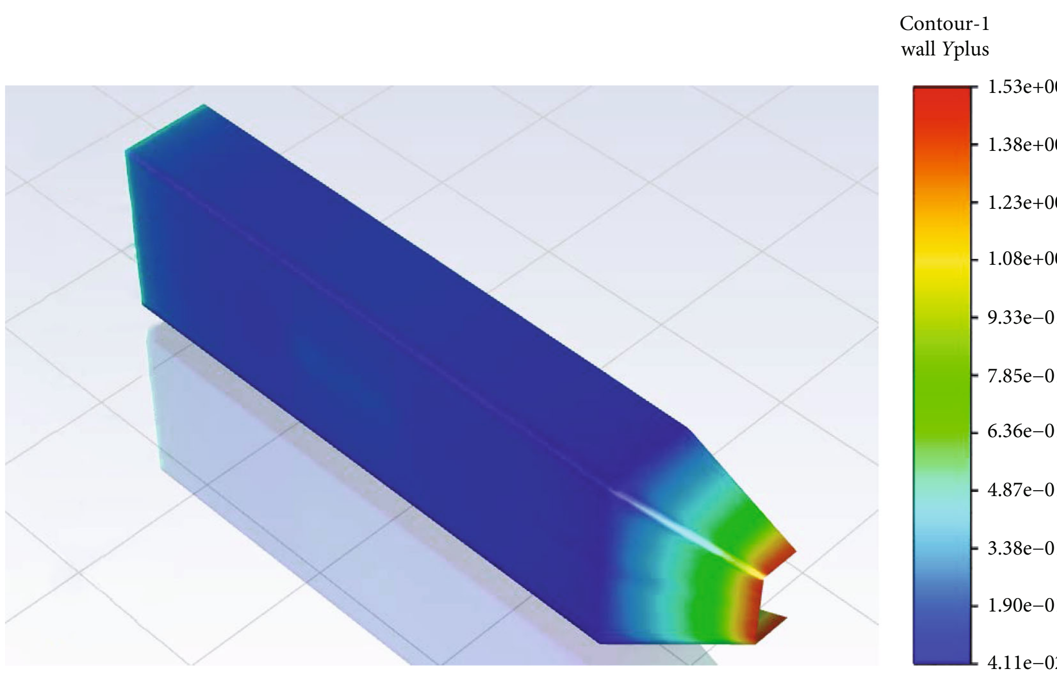

(b)

Figure 8: Wall Y^+ contour for (a) $k-\omega$ SST turbulence model and (b) realizable $k-\varepsilon$.

where Me is the equilibrium moisture content as obtained from the moisture sorption isotherm model defined in the modified Henderson sorption isotherm model.

Equation (20) and the modified Henderson model equation were written in a C-code including the constant values and compiled in ANSYS Fluent. The momentum source term including the permeability and inertial resistance factors (α, C_2) was determined from the Ergun equations [28] and found to be $6.924 \times 10^{-7}\,\mathrm{m}^2$ and $12924.6427\,\mathrm{m}^{-1}$, respectively. These factors were inserted in the momentum source term dialog box of ANSYS Fluent.

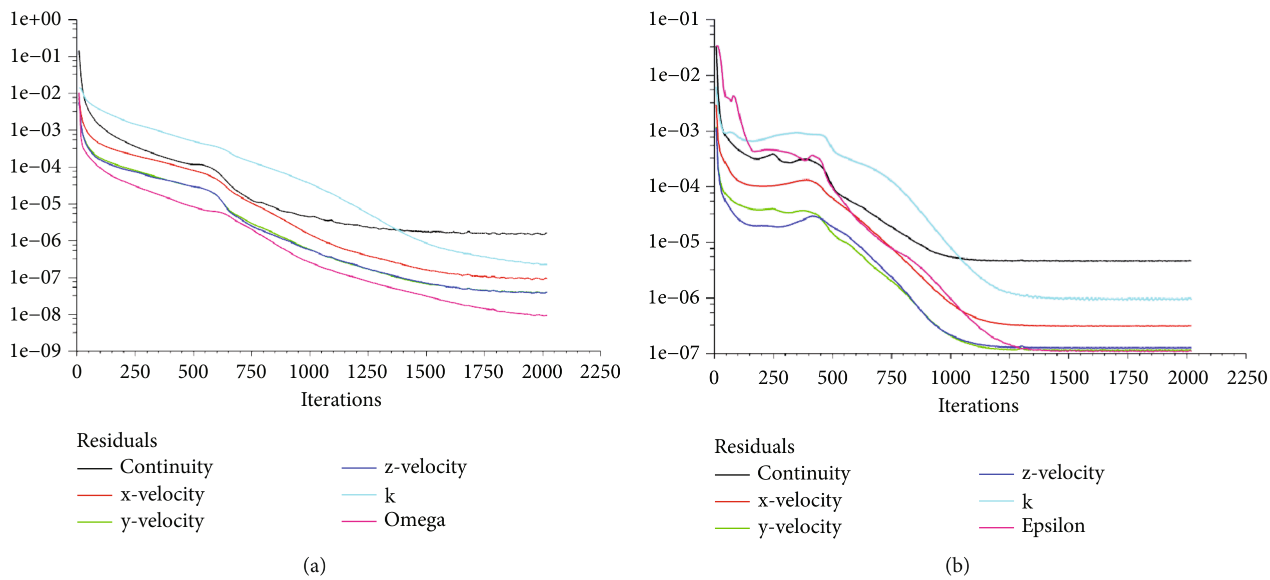

Figure 9: Plot of residuals for (a) $k-\omega$ SST turbulence model and (b) realizable $k-\mathcal{E}$ turbulence model.

3.3. Simulation of Mushroom Drying in a Tray Dryer

3.3.1. Geometry and Meshing. The simulation via ANSYS Fluent of moisture removal in the mushroom drying process was performed on an Intel Core i7 computer with 3.25 CPU and 16 GB RAM with 4 parallel processes and double precision calculations for about five hours.

(1) Geometry of the Tray Dryer. The actual tray dryer was converted into a computer-designed geometry using the given dimensions of the real dryer as shown in Figure 6. To reduce the simulation time and memory requirements, half of the dryer was considered in the simulations exploiting its symmetry.

(2) Grid Generation. The symmetrical 3D flow domain was discretized into a fine unstructured computational element (small volumes) by a meshing subprogram of ANSYS software. The generated grid has 1,075,142 elements and 362,144 nodes, with a maximum aspect ratio of 9.98 and a skewness of 0.89, which indicate a good mesh quality, as reported in [39]. The generated computational grid with inflation layer in the near wall is shown in Figures 7(a) and 7(b).

3.3.2. Solution and Simulation Results

(1) Flow Convergence. Y+: wall function approach: the flow of hot air in the dryer was simulated with two turbulence models (realizable $k-\mathcal{E}$ and $k-\omega$ SST). The $k-\omega$ SST model gave a maximum of 1.22 for wall $Y+$, whereas the realizable k-$\mathcal{E}$ model returns a maximum value of 1.53. The $k-\omega$ SST model resulted in better wall $Y+$ values. Therefore, the $k-\omega$ SST model has the capability of handling the flows in the near walls. The wall $Y+$ value for the viscous layer would be preferred less than five, better yet near to 1 [37]. In this case, both models gave a good result, and the $k-\omega$ SST model is converged fast with 2000 iterations and also selected since its value is nearer to one. Providing a suitable inflation mesh for the geometry is strongly tied to the choice of the turbulence model, and so, for a porous media, modelling with the $k-\omega$ SST turbulence model was preferred. The contour plot of wall $Y+$ values and the residual plot for both $k-\omega$ SST and realizable $k-\mathcal{E}$ are shown in Figures 8(a), 8(b), 9(a), and 9(b).

The convergence of the numerical simulations (in the absence of the source terms) was checked by the plots of the residual values and the solution imbalance between the inlet and outlet. The residual plots and the iterative values were less than 10^{-6} for velocities, turbulent kinetic energy, and dissipation rate and less than 10^{-5} for continuity in both turbulence models, as shown in Figure 9. The mass-flux net difference between the inlet and out was very small (-4.4×10^{-8}) and less than 1%. So, this indicates that the numerical simulation is so converged.

3.4. Results Obtained with the Inclusion of the Source Term and Postprocessing Analysis

3.4.1. Temperature Distribution. From the beginning of the tray dryer till near the sample, the temperature of the drying medium is fixed at the inlet temperature (60°C). After a short while, the hot air reached the porous zone, which is at the room temperature (25°C), and exchanges heat. The hot air can hold more moisture than the moist air, and so, the moisture in the sample is removed and reached at the equilibrium moisture content with a temperature of 57°C on the sample. The porous zone and drying air reach the same temperature within five hours, and the whole fluid domain shows a uniform temperature distribution with the porous zone (Figure 10(a)). At the end of the simulations, the minimum temperature (322 K) was observed at the near wall of the dryer. The temperature distribution on the sample (porous media) is shown in Figure 10(b). The temperature in the porous zone increases from the room

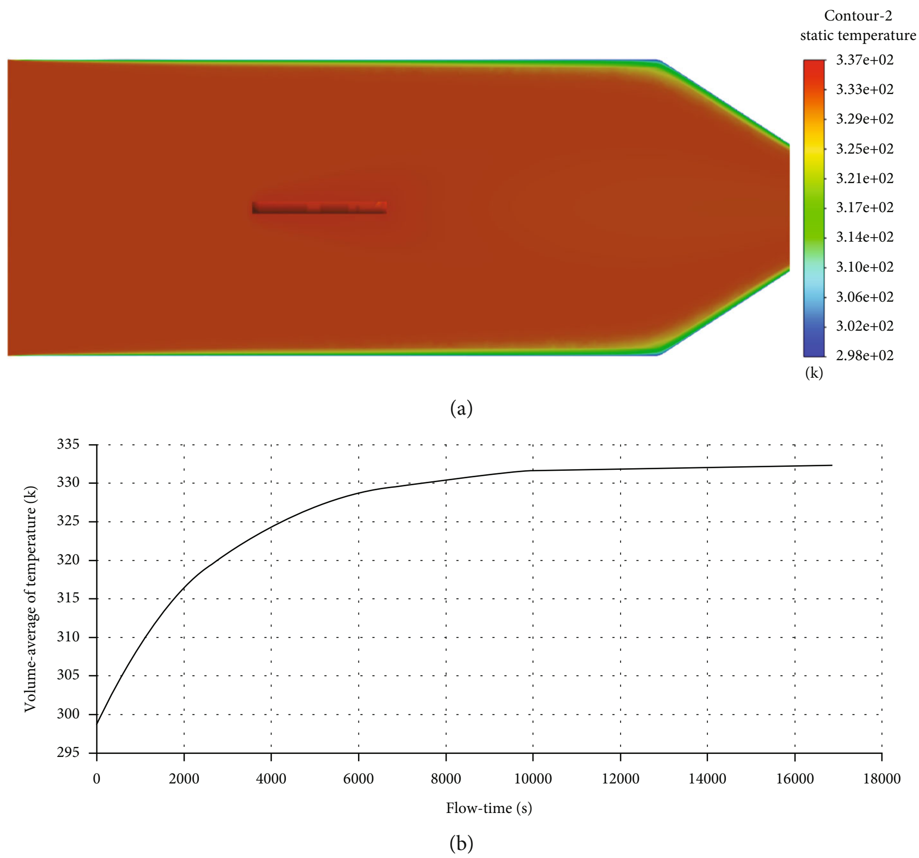

Figure 10: Temperature distribution (a) across the tray dryer on the symmetry plane and (b) on the porous zone after five hours.

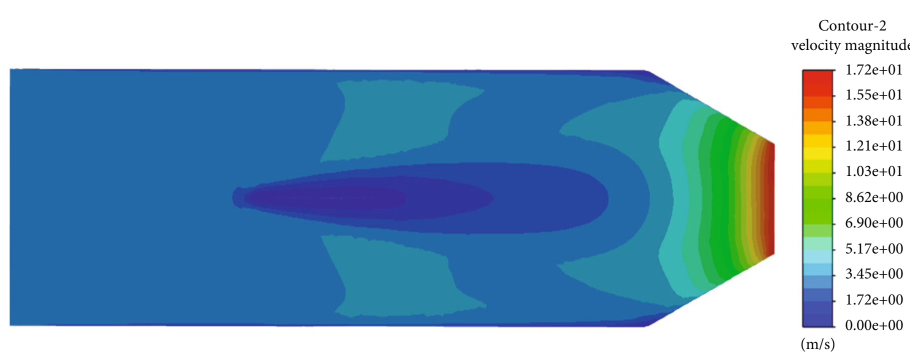

Figure 11: Velocity distribution of the drying air of the fluid domain on the symmetry plane at the end of simulations.

temperature of 330 K and then continued at a constant temperature of drying air (60°C).

3.4.2. Air Flow Predictions (Velocity Contour). The drying air velocity distribution in the drying unit has a significant effect on moisture removal from the sample. Figure 11 shows the air velocity magnitude in the symmetry plane. The maximum velocity (17.2 m/s) was observed at the exit of the tray dryer. The velocity profile from the inlet to the whole fluid domain is uniform (equal to 3 m/s), whereas it slows down (1 m/s) near and along the porous zone. It is clearly shown that on the forwards of the porous zone, the slowest airflow has happened. This is due to the viscous and inertial resistance of the porous media (mushroom).

3.4.3. Absolute Humidity Profile. The relative humidity profile (the UDS) contour plot is shown in Figure 12. The minimum absolute humidity of air at the inlet of the dryer was observed to be 12.8%. Then, when it came to the mushroom, it increased to 13.0%, which is the maximum observed. This is due to moisture transfer from the mushroom to the flowing air.

3.4.4. Pressure Contour. The pressure contour of the airflow in the symmetry plane of the dryer is presented in Figure 13. Its distribution is uniform along the dryer except for the

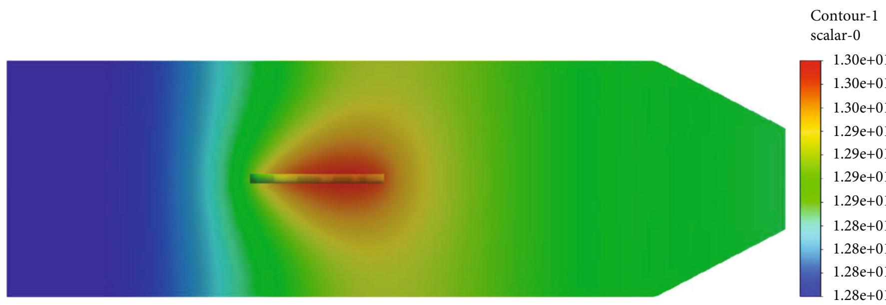

Figure 12: Relative humidity distribution on the symmetry plane at the end of simulation.

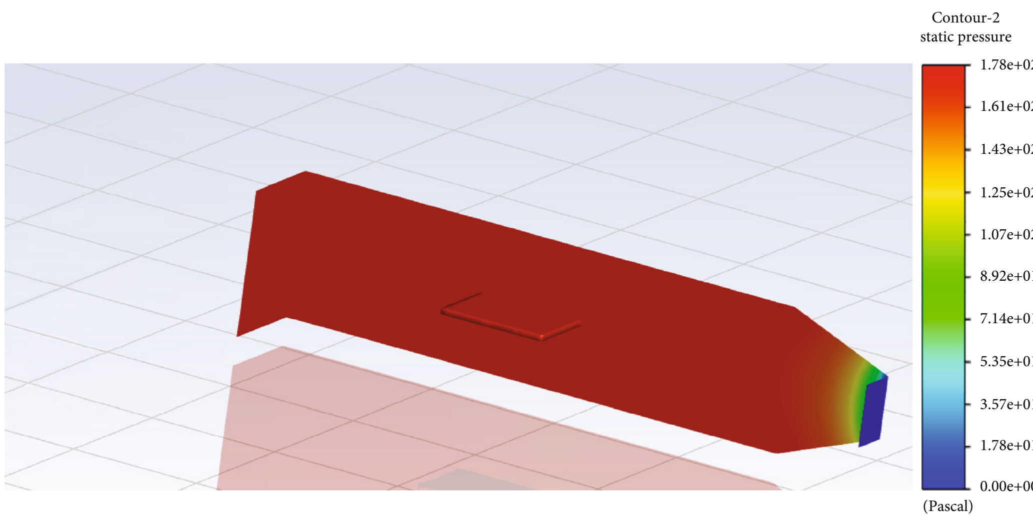

Figure 13: Pressure contour plot in the symmetry plane of the tray dryer.

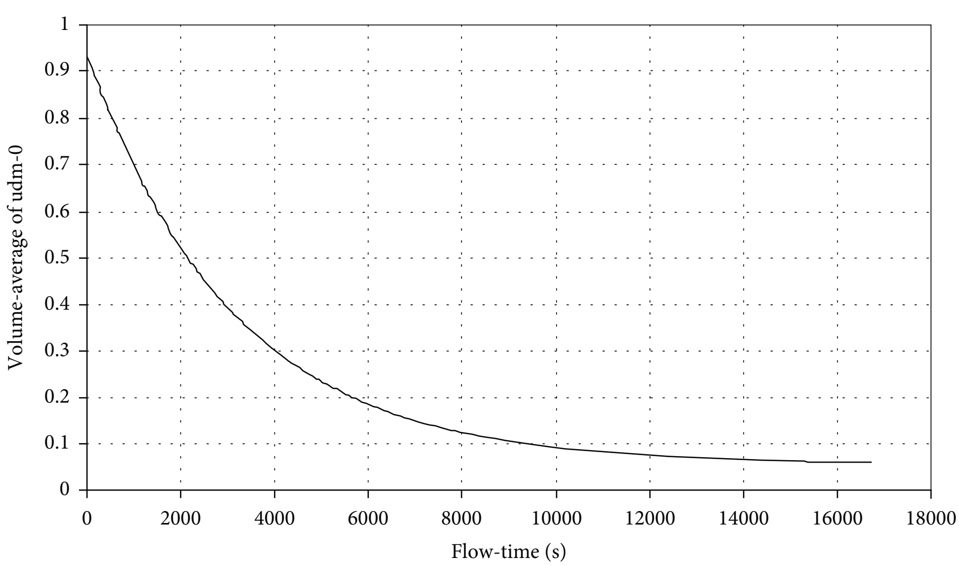

Figure 14: Moisture removal from the porous zone.

outlet section. The gauge static pressure at the exit of the dryer is approximately zero (equal to the pressure assumed in the outlet boundary condition). This is because the fluid velocity at the constriction is greater.

3.4.5. Moisture Removal from the Porous Media (Mushroom Drying). At the end of the simulation, the mushroom moisture content achieves around 5.7 wt% from the initial moisture content of 93.8 wt%. At the end of the simulation, 88.1%

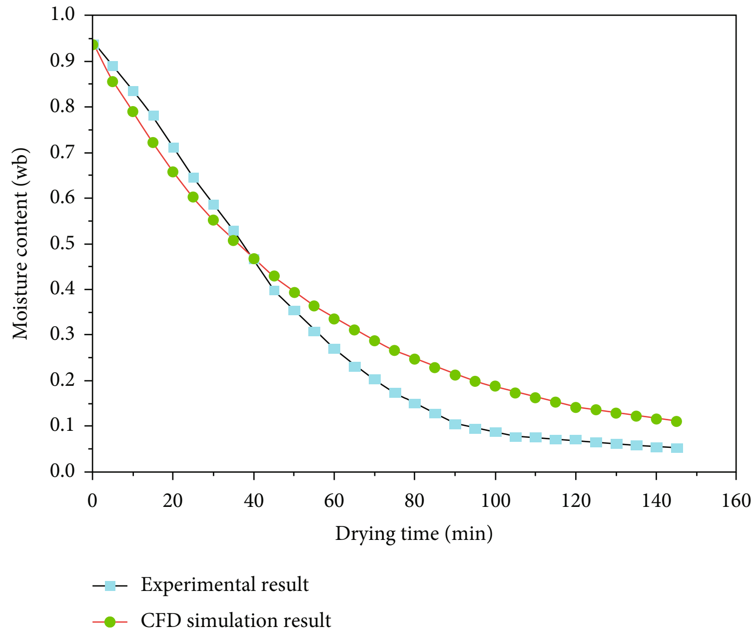

(a)

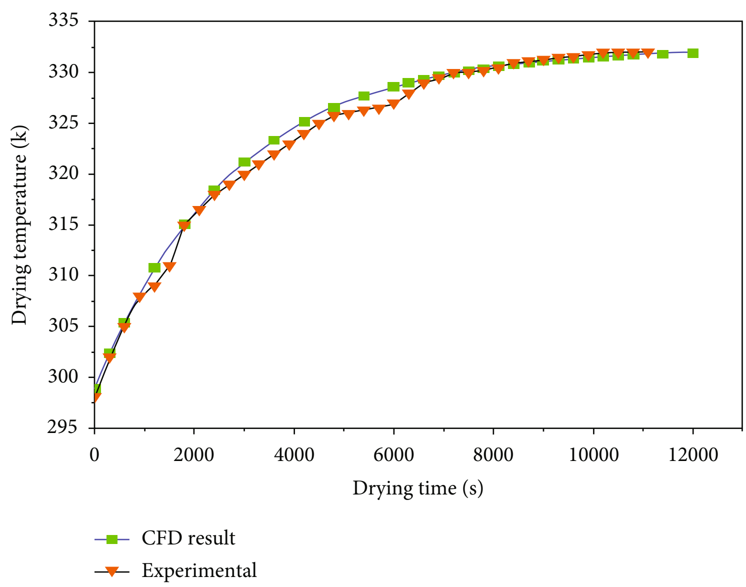

(b)

FIGURE 15: Continued.

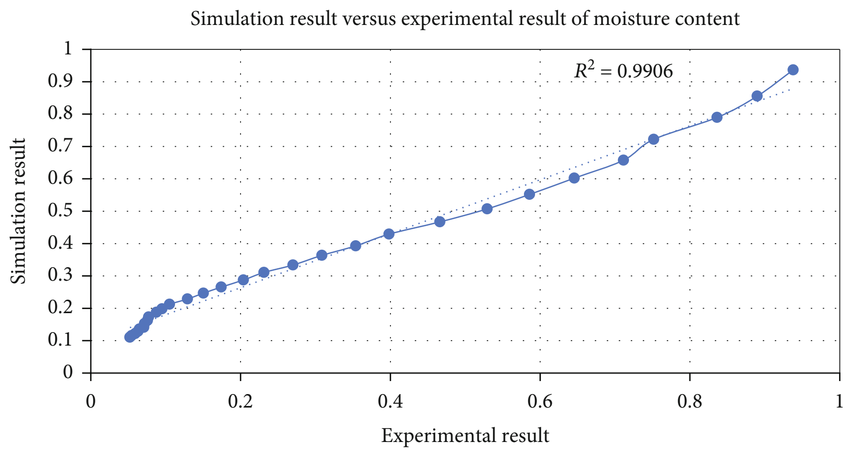

(c)

Figure 15: Comparison of experimental data with CFD simulation results. (a) Volume averaged moisture content time series, (b) air temperature time series, and (c) experimental moisture content vs. simulation moisture content.

of the moisture content of the mushroom was removed (Figure 14). This shows that the drying of mushroom was fast in the first hour, and then the constant period was observed after two and half hours. The final moisture content (5.7 wt%) observed in the simulation result was the nearest value to the moisture value found in the drying kinetics study at 60°C (5.21 wt%).

3.5. Validation of Simulation Results with the Experimental Value. The validation of the numerical results was done against the drying temperature and the moisture removal from the sample. The comparison of drying moisture content measured in the experiments with the CFD simulation results with drying time, and experimental vs. simulation results of moisture content are shown in Figures 15(a)–15(c). In Figure 15(a), it can reasonably be stated that the experimental result of the moisture content measured was well matched with the volume-averaged simulation result of the moisture content. Besides, the R^2 value of 0.9906 is a good indication that both simulation and experimental results were more or less similar to each other as illustrated in Figure 15(c). In a similar fashion, the distribution of drying temperature in the sample found during the experiment and simulation had a similar pattern as demonstrated in Figure 15(b). It is evident that the simulation of mushroom drying explains pretty well. The fitting of simulation and experimental results yielded R^2 value of 0.926.

However, a little deviation was observed in the volume average of simulated drying temperature and experimental data as well as in the moisture removal comparison as depicted in the plot (Figure 15(b)). This would be due to the loss of heat while measuring the temperature in the experiment and instrumental errors.

4. Conclusions

The drying model of mushroom drying and related parameters of the drying process were optimized using Design-Expert and found that 60°C drying temperature, 3 m/s air speed, and 200 g mass loading are the optimal values. At these optimum drying conditions, the moisture content of the mushroom sample was reduced from 93.8 to 5.7 wt% using a tray dryer. The drying kinetics analysis shows that Midilli et al.'s kinetic model was the best-fit model for oyster mushroom drying. The modified Henderson sorption's isotherm model was the best-fit model that relates *Me* of mushroom with its water activity. In combination with the kinetics and sorption models and applying the conservation equations of mass, momentum, and energy, a CFD-based model of a tray dryer for mushroom drying was developed. The source terms for the mass and heat were written in C-programs and compiled for the ANSYS Fluent solver. The drying process of mushrooms in a tray dryer was simulated in 3D. The results of the simulation (moisture content and drying temperature on the porous zone) were compared with the experimental results of moisture content and drying temperature, showing a good agreement with R^2 values of 0.99 and 0.93, respectively.

Generally, this work revealed that at the optimum drying conditions, CFD-based modelling and simulation are effective tools for describing mushroom or all other fruits drying in a tray dryer involving a continuous transfer of mass, momentum, and heat in a drying fluid flow. This is very important for many food industries and research institutes (laboratories) since it reduces the number of experiments which lowers operating costs and also saves more time. The mushrooms were sliced and taken as flat in this study, but some are spherical. To the best of our knowledge, dealing with simulations of this type has not yet been studied and could be considered in future work. Moreover, the physical parameters of the mushroom (thermal conductivity, density, and heat capacity) are all taken as constant. For instance, these parameters could be assumed as a function of moisture content and temperature to lower the deviation observed in the validation.

Nomenclature

AH:	Absolute humidity
a_w:	Water activity
hr., min, s:	Hour, minute, second, respectively
t:	Time
k:	Turbulent kinetic energy
MC:	Moisture content
MR:	Moisture ratio
M_t:	Moisture content at time t
M_0:	Initial moisture content
Me:	Equilibrium moisture content
P_{sat}:	Saturation pressure
RH:	Relative humidity
T_{abs}:	Absolute temperature
UDF/UDS:	User-defined-function/user-defined-scalars
wt:	Weight
R^2:	Coefficient of determination
D_{eff}:	Effective moisture diffusivity
D_{ef}:	Effective diameter
ρ:	Density of the fluid
$\vec{V}$:	Velocity vector
μ:	Dynamic viscosity
Cp:	Specific heat capacity at constant pressure
S_m, S_i, S_h:	Source term for mass, momentum, and energy equation
ρ:	Fluid density
ϕ:	Any variant (velocity, components, and enthalpy)
s_ϕ:	Source term of any property variant
α:	Permeability of the medium
C_2:	The pressure-jump coefficient
$Y+$:	Wall functions or wall distance estimation
3D; 2D:	Three dimensional; two dimensional.

Data Availability

The data used to support the findings of this study are included in the article and supplementary file. Anyone looking for any data can contact the corresponding author or first author upon reasonable request.

Conflicts of Interest

The authors declare that they have no known competing financial interests or personal relationships that could have appeared to influence the work reported in this paper.

Authors' Contributions

Talbachew Tadesse Nadew was responsible for the conceptualization, methodology, formal analysis, investigation, writing—original draft preparation, data curation reviewing, and C-coding. Tsegaye Sissay Tedila was responsible for the writing—review and supervision, visualization, and editing. Petros Demissie Tegenaw was responsible for the software, validation, visualization, reviewing, and supervision. All authors have read and agreed to publish this version of the manuscript.

Acknowledgments

The authors would like to thank the Department of Chemical Engineering, College of Food and Chemical Engineering, Wollo University, Kombolcha Institute of Technology, Kombolcha, Ethiopia, and Addis Ababa Science Technology University, Addis Ababa, Ethiopia, for their collaboration during the laboratory work.

Supplementary Materials

UDF is a C-code function that can be dynamically loaded with the ANSYS Fluent solver to enhance moisture transport phenomena. The C-code written on *Code:: Blocks* include the DEFINE macros, flow variable macros, user-defined scalar and memory macros, and looping macros. The definition of constants and initial values was defined using DEFINE_INIT macros. The mushroom moisture content update at each time step for each computational cell according to the temperature and absolute humidity of intergranular air was defined using DEFINE_ADJUST macros. The mass and energy source term calculation and return to the solver were introduced using DEFINE_SOURCE macros. The solution iteration loop begins with the execution of ADJUST UDFs. Then, ANSYS Fluent solves the governing equations of continuity, momentum, and energy transport in a coupled fashion. *(Supplementary Materials)*

References

[1] K. Kaur, S. Kumar, and M. S. Alam, "Air drying kinetics and quality characteristics of oyster mushroom (*Pleurotus ostreatus*) influenced by osmotic dehydration," *Agricultural Engineering International: CIGR Journal*, vol. 16, no. 3, pp. 214–222, 2014.

[2] E. Demiray, "Drying characteristics and kinetics of lovastatin degradation of oyster mushroom (*Pleurotus Ostreatus*) slices," *Latin American Applied Research-An International Journal*, vol. 49, no. 4, pp. 269–274, 2019.

[3] K. Zhang, Y.-Y. Pu, and D.-W. Sun, "Recent advances in quality preservation of postharvest mushrooms (*Agaricus bisporus*): a review," *Trends in Food Science and Technology*, vol. 78, pp. 72–82, 2018.

[4] C. Toledo, C. Barroetaveña, Â. Fernandes, L. Barros, and I. Ferreira, "Chemical and antioxidant properties of wild edible mushrooms from native Nothofagus spp. forest, Argentina," *Molecules*, vol. 21, no. 9, p. 1201, 2016.

[5] T. Arumuganathan, M. R. Manikantan, R. D. Rai, S. Anandakumar, and V. Khare, "Mathematical modeling of drying kinetics of milky mushroom in a fluidized bed dryer," *International Agrophysics*, vol. 23, no. 1, pp. 1–7, 2009.

[6] N. N. Potter and J. H. Hotchkiss, "Unit operations in food processing," in *Food Science Text Series*, pp. 69–89, Pergamon press, 1995.

[7] K. Sattler and H. J. Feindt, *Thermal Separation Processes*, Wiley, 1995.

[8] I. Tinebra, R. Passafiume, D. Scuderi et al., "Effects of tray-drying on the physicochemical, microbiological, proximate, and sensory properties of white- and red-fleshed loquat (*Eriobotrya Japonica Lindl.*) fruit," *Agronomy*, vol. 12, no. 2, p. 540, 2022.

[9] S. Piskov, L. Timchenko, W. D. Grimm et al., "Effects of various drying methods on some physico-chemical properties and the antioxidant profile and ACE inhibition activity of oyster mushrooms (Pleurotus ostreatus)," *Foods*, vol. 9, no. 2, p. 160, 2020.

[10] E. Tsotsas, T. Metzger, V. Gnielinski, and E.-U. Schlünder, *Drying of Solid Materials*, Ullmann's Encycl. Ind. Chem, 2010.

[11] S. Misha, S. Mat, M. H. Ruslan, K. Sopian, and E. Salleh, "Review on the application of a tray dryer system for agricultural products," *World Applied Sciences Journal*, vol. 22, no. 3, pp. 424–433, 2013.

[12] C. T. Kiranoudis, Z. B. Maroulis, D. Marinos-Kouris, and M. Tsamparlis, "Modeling and optimization of a tunnel crape dryer," *Drying Technology*, vol. 14, no. 7–8, pp. 1695–1718, 1996.

[13] S. Rafiee and E. Meisami-asl, "Mathematical modeling of kinetics of thin-layer drying of apple (var. Golab)," *Agricultural Engineering International: CIGR Journal*, vol. XI, 2009.

[14] R. P. Kingsly, R. K. Goyal, M. R. Manikantan, and S. M. Ilyas, "Effects of pretreatments and drying air temperature on drying behaviour of peach slice," *International Journal of Food Science and Technology*, vol. 42, no. 1, pp. 65–69, 2007.

[15] K. Górnicki and A. Kaleta, "Drying curve modelling of blanched carrot cubes under natural convection condition," *Journal of Food Engineering*, vol. 82, no. 2, pp. 160–170, 2007.

[16] R. A. Chayjan, M. H. Peyman, M. Esna-Ashari, and K. Salari, "Influence of drying conditions on diffusivity, energy and color of seedless grape after dipping process," *Australian Journal of Crop Science*, vol. 5, no. 1, pp. 96–103, 2011.

[17] H. F. Oztop and E. K. Akpinar, "Numerical and experimental analysis of moisture transfer for convective drying of some products," *International Communications in Heat and Mass Transfer*, vol. 35, no. 2, pp. 169–177, 2008.

[18] G. P. Apati, S. A. Furlan, and B. J. Laurindo, "Drying and rehydration of oyster mushroom," *Brazilian Archives of Biology and Technology*, vol. 53, no. 4, pp. 945–952, 2010.

[19] A. Bakker, A. H. Haidari, and L. M. Oshinowo, "Realize greater benefits from CFD," *Chemical Engineering Progress*, vol. 97, no. 3, pp. 45–53, 2001.

[20] R. P. Ramachandran, M. Akbarzadeh, J. Paliwal, and S. Cenkowski, "Computational fluid dynamics in drying process modelling—a technical review," *Food and Bioprocess Technology*, vol. 11, no. 2, pp. 271–292, 2018.

[21] L. Wu, K. Yick, S. Ng, and J. Yip, "Application of the Box–Behnken design to the optimization of process parameters in foam cup molding," *Expert Systems with Applications*, vol. 39, no. 9, pp. 8059–8065, 2012.

[22] G. K. Uyanık and N. Güler, "A study on multiple linear regression analysis," *Procedia - Social and Behavioral Sciences*, vol. 106, pp. 234–240, 2013.

[23] G. R. Thorpe, "The application of computational fluid dynamics codes to simulate heat and moisture transfer in stored grains," *Journal of Stored Products Research*, vol. 44, no. 1, pp. 21–31, 2008.

[24] M. Ranjbaran, B. Emadi, and D. Zare, "CFD simulation of deep-bed paddy drying process and performance," *Drying Technology*, vol. 32, no. 8, pp. 919–934, 2014.

[25] T. D. Canonsburg, *ANSYS Fluent User's Guide, vol. 15317, no. 15.0*, ANSYS, Inc., USA, 2013.

[26] A. K. Coker, *Fortran Programs for Chemical Process Design, Analysis, and Simulation*, Elsevier Science & Technology Books, 1995.

[27] R. B. Bird, "Transport phenomena," *Applied Mechanics Reviews*, vol. 55, no. 1, pp. R1–R4, 2002.

[28] S. Ergun, "Fluid flow through packed column," in *Fluid Mechanics*, p. 89, Carnegie Institute of Technology, Pittsburgh, pennsylvania, 2003.

[29] D. Zare, H. Naderi, and M. Ranjbaran, "Energy and quality attributes of combined hot-air/infrared drying of paddy," *Drying Technology*, vol. 33, no. 5, pp. 570–582, 2015.

[30] G. Pavan-Melendez, "Dimensionless analysis of the simultaneous heat and mass transfer in food drying," *Journal of Food Engineering*, vol. 51, no. 4, pp. 347–353, 2002.

[31] B. Mahayothee, T. Thamsala, P. Khuwijitjaru, and S. Janjai, "Effect of drying temperature and drying method on drying rate and bioactive compounds in cassumunar ginger (*Zingiber montanum*)," *Journal of Applied Research on Medicinal and Aromatic Plants*, vol. 18, article 100262, 2020.

[32] İ. Doymaz, "Drying kinetics and rehydration characteristics of convective hot-air dried white button mushroom slices," *Journal of Chemistry*, vol. 2014, Article ID 453175, 8 pages, 2014.

[33] Y. Tulek, "Drying kinetics of oyster mushroom (Pleurotus ostreatus) in a convective hot air dryer," *Journal of Agricultural Science and Technology*, vol. 13, no. 5, pp. 655–664, 2011.

[34] P. Udomkun, D. Argyropoulos, M. Nagle, B. Mahayothee, S. Janjai, and J. Müller, "Single layer drying kinetics of papaya amidst vertical and horizontal airflow," *LWT - Food Science and Technology*, vol. 64, no. 1, pp. 67–73, 2015.

[35] S. Basu, U. S. Shivhare, and A. S. Mujumdar, "Models for sorption isotherms for foods: a review," *Drying Technology*, vol. 24, no. 8, pp. 917–930, 2006.

[36] M. M. Abbott and V. Ness, *Introduction to Chemical Engineering Thermodynamics*, Boston Burr Ridge, Singapore: McGraw-Hill, 6th edition, 2001.

[37] S. C. Salim and M. Salim, "Wall Y+ plus strategy for dealing with wall-bounded turbulent flows," *An Introduction to Computational Fluid Dynamics*, vol. II, p. 72, 2009.

[38] S. Varga, A. C. Oliveira, X. Ma, S. A. Omer, W. Zhang, and S. B. Riffat, "Comparison of CFD and experimental performance results of a variable area ratio steam ejector," *International Journal of Low-Carbon Technologies*, vol. 6, no. 2, pp. 119–124, 2011.

[39] J. Park and S. M. Shontz, "An alternating mesh quality metric scheme for efficient mesh quality improvement," *Procedia Computer Science*, vol. 4, pp. 292–301, 2011.

[40] K. Agbossou, K. Napo, and S. Chakraverty, "Mathematical modelling and solar tunnel drying characteristics of yellow maize," *American Journal of Food Science and Technology*, vol. 4, no. 4, pp. 115–124, 2016.

[41] O. Yaldiz, C. Ertekin, and H. I. Uzun, "Mathematical modeling of thin layer solar drying of sultana grapes," *Energy*, vol. 26, no. 5, pp. 457–465, 2001.

[42] O. Yaldýz and C. Ertekýn, "Thin layer solar drying of some vegetables," *Drying Technology*, vol. 19, no. 3–4, pp. 583–597, 2001.

[43] S. M. Henderson, "Progress in developing the thin layer drying equation," *Transactions of the ASAE*, vol. 17, no. 6, pp. 1–3, 1974.

[44] S. Kumar, S. S. Mahanand, and P. Kumar, "Mathematical modelling and experimental analysis of broccoli (*Brassica*

oleracea I.) in tray dryer," *Journal of Pharmacognosy and Phytochemistry*, vol. 6, no. 6, pp. 1049–1052, 2017.

[45] A. Midilli, H. Kucuk, and Z. Yapar, "A new model for single-layer drying," *Drying Technology*, vol. 20, no. 7, pp. 1503–1513, 2002.

[46] U. E. Inyang, I. O. Oboh, and B. R. Etuk, "Kinetic models for drying techniques-food materials," *Advances in Chemical Engineering and Science*, vol. 8, no. 2, pp. 27–48, 2018.

[47] D. S. Chung and H. B. Pfost, "Adsorption and desorption of water vapor by cereal grains and their products part III: a hypothesis for explaining the hysteresis effect," *Transactions of the ASAE*, vol. 10, no. 4, pp. 0556-0557, 1967.

[48] R. Boquet, J. Chirife, and H. A. Iglesias, "Equations for fitting water sorption isotherms of foods," *International Journal of Food Science and Technology*, vol. 13, no. 4, pp. 319–327, 1978.

[49] S. Henderson, "A mean moisture content-equilibrium relative humidity relationship for nine varieties of wheat," *Journal of Stored Products Research*, vol. 23, no. 3, pp. 143–147, 1987.

[50] C. Berg, "Development of B.E.T.-like models for sorption of water on foods, theory and relevance," in *Properties of Water in Foods*, J. L. M. D. Simatos, Ed., pp. 119–131, Springer Netherlands, Dordrecht, 1985.

[51] J.-F. Pommaret, "Adsorption of gases in multimolecular layers," in *Partial Differential Equations and Group Theory, vol. 407, no. 1*, pp. 61–80, Springer Netherlands, Dordrecht, 1994.

[52] F. C. Tompkins, "Physical adsorption on non-uniform surfaces," *Transactions of the Faraday Society*, vol. 46, no. 2012, p. 569, 1950.

[53] C. F. Fontan, J. Chirife, E. Sancho, and H. A. Iglesias, "Analysis of a model for water sorption phenomena in foods," *Journal of Food Science*, vol. 47, no. 5, pp. 1590–1594, 1982.